

RSC Advances



This is an *Accepted Manuscript*, which has been through the Royal Society of Chemistry peer review process and has been accepted for publication.

Accepted Manuscripts are published online shortly after acceptance, before technical editing, formatting and proof reading. Using this free service, authors can make their results available to the community, in citable form, before we publish the edited article. This *Accepted Manuscript* will be replaced by the edited, formatted and paginated article as soon as this is available.

You can find more information about *Accepted Manuscripts* in the [Information for Authors](#).

Please note that technical editing may introduce minor changes to the text and/or graphics, which may alter content. The journal's standard [Terms & Conditions](#) and the [Ethical guidelines](#) still apply. In no event shall the Royal Society of Chemistry be held responsible for any errors or omissions in this *Accepted Manuscript* or any consequences arising from the use of any information it contains.

Production of aqueous dispersions of inorganic graphene analogues by exfoliation and stabilization with non-ionic surfactants

Laura Guardia^{*}, Juan I. Paredes, Rubén Rozada, Silvia Villar-Rodil, Amelia Martínez-Alonso, Juan M. D. Tascón

Instituto Nacional del Carbón, INCAR-CSIC, Apartado 73, 33080 Oviedo, Spain

Abstract

The production of stable aqueous suspensions of several inorganic graphene analogues [MoS₂, WS₂ and hexagonal BN (h-BN)] by exfoliation of the corresponding bulk layered materials via sonication has been investigated, with a particular focus on the use and efficacy of non-ionic surfactants as dispersing agents. For the two metal dichalcogenides, some non-ionic surfactants afforded highly concentrated dispersions (up to several milligrams per milliliter), outperforming dispersions produced with an ionic surfactant or in water-alcohol mixtures in the absence of surfactant, which were taken as reference systems. Furthermore, suspensions with metal dichalcogenide to surfactant concentration ratios as high as 2.4 – 3.5 could be attained through appropriate processing of the as-prepared suspensions, which should be advantageous for the preparation of materials and devices with minimal interference from the surfactant. In the case of h-BN, all surfactants failed to yield suspensions with concentration significantly above that achieved in water alone, which was attributed to the chemical peculiarities of h-BN platelets exfoliated in water via sonication. The suspensions produced with the most successful non-ionic surfactants exhibited long-term stability (months) and were made up of platelets with lateral dimensions from 50 up to a few

^{*} Corresponding author: Telephone number: (+34) 985 11 90 90. Fax number: (+34) 985 29 76 62. E-mail address: lauraguardia@incar.csic.es (L.Guardia)

hundred nanometers and thicknesses of a few to several nanometers. Raman spectroscopy analysis suggested that edge effects dominate the detailed spectral features for the MoS₂ and WS₂ platelets, in particular the position of their Raman bands. Such result indicates that extreme caution must be exercised when using this technique to gauge the thickness of small-sized MoS₂/WS₂ platelets, such as those typically produced by liquid-phase exfoliation approaches. Overall, the present results should facilitate the manipulation and use of these two-dimensional materials in several prospective applications areas, such as biomedicine or photocatalysis.

1. Introduction

During the last decade, research on graphene has progressed at a breathtaking pace in a number of fronts that encompass its production, fundamental science and prospective applications.^{1,2} Such efforts have been mainly driven by the exceptional electronic, mechanical, thermal and optical properties of this carbon material, and also by the observation of exotic physical phenomena related to its two-dimensional (2D) nature.^{1,3} As a direct consequence of the explosion of activity in the graphene field, interest in other 2D materials has been steadily growing over the last few years.⁴⁻⁸ These are quite numerous and include layered transition metal dichalcogenides (e.g., MoS₂ and WS₂) and other metal chalcogenides (GaSe, Bi₂Te₃, etc), layered transition metal oxides (MnO₂, Nb₃O₈, etc), as well as hexagonal boron nitride (h-BN), silicene and germanene.^{4,5} Single- and few-layer sheets of such materials are expected to exhibit outstanding physical properties and can therefore complement graphene in the development of novel materials and devices for use in many areas, including electronics, photonics, sensing, energy conversion and storage, biomedicine or catalysis.⁴⁻⁸

Similar to the case of graphene, the large-scale implementation of 2D materials in practical applications will only be possible if cost-effective methods for their mass production and processing become available.^{9,10} In this regard, as has already been demonstrated with graphene,¹¹ top-down approaches based on the exfoliation of bulk layered crystals in the liquid phase are in principle one of the most attractive routes to access 2D materials in large quantities.¹² Such approaches would afford colloidal dispersions of the 2D sheets and readily lend themselves to the preparation of, e.g., inks, thin films, composites and hybrid materials.

Many layered crystals, particularly transition metal dichalcogenides, can be efficiently exfoliated by means of a lithium intercalation process that yields aqueous colloidal dispersions of single-layer sheets.¹³⁻¹⁶ However, this method is extremely environment-sensitive and can lead to structural and electronic changes in the sheets as a result of the intercalation step.^{13,16} Alternatively, layered compounds can be directly exfoliated in certain solvents with the assistance of ultrasound.¹⁷ In this case, exfoliation and stabilization of the 2D sheets has been shown to be favored in solvents with surface energies roughly matching that of the dispersed material.^{17, 18} Typical successful solvents of many 2D materials include several pyrrolidone derivatives (e.g., *N*-methyl-2-pyrrolidone), γ -butyrolactone and cyclohexanone, but unfortunately not water, which is often the preferred dispersing medium and the one required for their prospective use in, e.g., biomedical applications. Nevertheless, such drawback can be overcome with the aid of suitable dispersants. As a matter of fact, recent work has demonstrated that a number of surfactants are able to stabilize exfoliated sheets of several layered compounds in aqueous medium.¹⁹⁻²²

Notwithstanding the progress achieved so far in the surfactant stabilization of 2D sheets, this research area is still in its infancy and several issues have yet to be

addressed to take full advantage of aqueous dispersions of these novel materials. One of such issues relates to the fact that earlier efforts have mostly relied on ionic surfactants to stabilize the sheets,¹⁹⁻²² even though the use of non-ionic dispersants could potentially offer a number of benefits. For example, previous research on graphene has demonstrated that non-ionic surfactants tend to outperform ionic ones in terms of attaining high concentrations of dispersed material, which is always advantageous with a view to applications.^{23,24} Similar trends might apply with other 2D materials, but to the best of our knowledge this question has not been examined in detail. Likewise, in biomedical research non-ionic surfactants are frequently the dispersants of choice on biocompatibility grounds,²⁴ so the availability of aqueous suspensions of 2D sheets stabilized by such type of surfactants would be highly desirable.

Therefore, in the present work we have investigated a suite of non-ionic surfactants regarding their ability to exfoliate under ultrasound and stabilize in aqueous medium 2D sheets of several layered compounds, namely, MoS₂ and WS₂ and h-BN. For the two metal chalcogenides, several efficient surfactants have been identified that afford significantly larger concentrations of these 2D sheets (up to several milligrams per milliliter) than it was previously possible in aqueous medium. The effect of several processing parameters, including initial concentration of layered material, surfactant concentration, as well as sonication time and power, has also been studied. On the other hand, the results reveal h-BN to be in a league of its own. It has been reported that this material can be exfoliated and dispersed in water in the absence of stabilizers through sonication-induced hydrolysis,²⁵ and it was expected that the use of surfactants would afford significant increases in the dispersed concentrations, but the results indicated that this is not the case.

2. Experimental

The starting layered materials MoS₂ and WS₂ as well as all the surfactants were purchased from Sigma-Aldrich and used as received, whereas h-BN was obtained from ESK Ceramics GmbH. The following non-ionic surfactants were tested: polyoxyethylene sorbitan monooleate (Tween 80), polyoxyethylene sorbitan trioleate (Tween 85), polyvinylpyrrolidone (PVP), polyoxyethylene (4) dodecyl ether (Brij 30), polyoxyethylene (100) octadecyl ether (Brij 700), polyoxyethylene octyl (9-10) phenyl ether (Triton X-100), gum arabic from acacia tree, Pluronic P-123 and n-dodecyl β-D-maltoside (DBDM). For comparison purposes, the anionic surfactant sodium cholate (SC), which has been reported to be an efficient dispersant of these materials,¹⁹ was also employed. In a typical dispersion experiment, the layered material was added at a given initial concentration (typically 30 mg mL⁻¹) to an aqueous surfactant solution and sonicated in a custom-made, variable power ultrasound bath cleaner (40 kHz, ATU Ultrasonidos S.L.) at a power of 26 W L⁻¹. The resulting suspension was typically centrifuged at 1500 rpm for 20 min in an Eppendorf 5424 microcentrifuge to sediment unexfoliated particles of the layered material and the top ~75 % of the supernatant volume was collected and stored for further characterization. The effect of surfactant concentration as well as sonication time and power, which could be varied from ~10 to 50 W L⁻¹, was investigated.

To evaluate and compare the effect of the different surfactants and processing conditions on the amount of layered material that was exfoliated and stably suspended in aqueous medium, UV-vis absorption spectroscopy was used. Spectra of the surfactant-stabilized dispersions were recorded on a double-beam Helios α spectrophotometer (Thermo Spectronic) in the 200-1000 nm wavelength range. In principle, both the surfactants and the exfoliated sheets could contribute to the observed

spectral features. In practice, only those surfactants with C=C bonds in their structure (e.g., Triton X-100) exhibited absorbance in such a range, but it was just limited to wavelengths below ~300 nm, the absorbance measured at longer wavelengths being exclusively brought about by the exfoliated sheets. Therefore, determination of the suspension absorbance at a given wavelength ≥ 300 nm can be used to estimate, at least in relative terms, the concentration of dispersed material. Here, such concentration was gauged by measuring absorbance at the following wavelengths: 350 nm (h-BN), 674 nm (MoS₂) and 630 nm (WS₂). We note, however, that similar to earlier reports, a significant background was observed in the spectra recorded for these materials, which was attributed to scattering of light by the sheets.¹⁷ The scattering background displayed an exponential wavelength dependence ($A \propto \lambda^{-n}$, where A is the measured absorbance, λ is the wavelength and n is the scattering exponent) that became more clearly evident in the non-resonant region at long absorption wavelengths (see below). Furthermore, because the magnitude of this background (i.e., the exponent n) is thought to depend on the sheet size, a meaningful comparison of the suspension concentrations achieved using different processing conditions (e.g., different sonication power and/or time) can in principle only be made after background subtraction. Such operation was indeed routinely carried out for all MoS₂ and WS₂ dispersions. However, we note that the background subtraction procedure can be a tricky task. For that reason, we implemented a procedure that was identical for either all MoS₂ or all WS₂ dispersions. Using the same subtraction routine for a given material (MoS₂ or WS₂) ensured the internal consistency of our results, although such results would probably not be directly comparable with those obtained using different subtraction routines. Specifically, because we measured absorbance values at 674 nm for MoS₂, we determined and subtracted the scattering background in the 730-955 nm region for dispersions of such

material; for WS₂ we measured absorbance values at 630 nm, so the background was determined and subtracted in the 710-950 nm region. We also note that h-BN is a large bandgap (~6 eV) semiconductor, so it only exhibits absorption at short wavelengths (below ~200 nm). Therefore, the signals measured in the UV-vis spectra at longer wavelengths should be exclusively due to scattering of light by the sheets and not to absorption. For this reason, h-BN concentrations could only be estimated using such background signal. However, because the lateral size of the h-BN sheets was very similar for dispersions prepared here under identical sonication conditions (i.e., power and time), the values obtained from the background signals should reflect their relative concentrations, and hence comparisons between different dispersions could be reasonably made. To obtain meaningful sets of data, the dispersions were prepared at least in triplicate, so that average and standard deviation values of absorbance can be provided.

Further characterization of the samples was accomplished by field emission scanning electron microscopy (FE-SEM), transmission electron microscopy (TEM), atomic force microscopy (AFM), Raman spectroscopy, X-ray photoelectron spectroscopy (XPS) and thermogravimetric analysis (TGA). FE-SEM was carried out on a Quanta FEG 650 apparatus (FEI Company). TEM images were recorded with a JEOL 2000 EX-II instrument operated at 160 kV. Samples for TEM were prepared by drop-casting ~20 µL of the surfactant-stabilized dispersions onto a Cu grid (200 mesh) covered with a continuous carbon film, which was then allowed to dry under ambient conditions. AFM was performed in the tapping mode of operation with a Nanoscope IIIa Multimode apparatus (Veeco Instruments), using rectangular Si cantilevers with spring constant of ~40 N m⁻¹ and resonance frequency around 250-300 kHz. To this end, the dispersions were drop-cast (~50 µL) onto either highly oriented pyrolytic graphite

(HOPG) or mica substrates pre-heated at ~50-60 °C. After drying, the substrates were thoroughly rinsed with Milli-Q water to remove surfactant from their surface. Raman spectra were obtained on a Horiba Jobin-Yvon LabRam instrument at a laser excitation wavelength of 532 nm. To avoid damage to the samples during the measurement, the power of the incident laser was kept to ~0.5 mW. XPS was performed on a SPECS spectrometer using a Mg K α X-ray source (1253.6 eV, 100 W) and working at a pressure of 10⁻⁷ Pa. The charge effect observed during analysis on h-BN was counteracted by the use of an electron flood gun. Specimens for both Raman spectroscopy and XPS were prepared by depositing the dispersions drop-wise onto a pre-heated flat metallic disk (12 mm in diameter) until a uniform film was seen to cover the substrate. The starting bulk MoS₂, WS₂ and h-BN samples were pressed into pellets with a hydraulic press. ATR-FTIR spectra were acquired with a Nicolet 8700 spectrometer, from Thermo Scientific, using diamond as ATR crystal. For TGA, an SDT Q600 thermobalance (TA Instruments) was employed. Thermograms were recorded under synthetic air flow (100 mL min⁻¹) at a heating rate of 3 °C min⁻¹, using Pt crucibles.

3. Results and discussion

In principle, the amount of layered material that can be exfoliated and stabilized in aqueous medium, as well as the characteristics of the resulting dispersions, are expected to depend on many processing parameters, including initial concentration and particle size of the layered compound, surfactant type and concentration, sonication time and power, and centrifugation conditions (time and centrifugal force). Among these, the initial concentration and particle size of the layered material are thought to be particularly relevant factors, because they should determine the amount of thin flakes

that are cleaved from the particles to be potentially stabilized by the surfactant molecules. Fig. 1 shows representative FE-SEM images of the starting h-BN (a), MoS₂ (b), and WS₂ (c) powders. Consistent with their layered nature, the materials are made up of thin particles, or plates, which display lateral sizes typically between 1 and 20 μm. For these powders, preliminary experiments with several surfactants indicated that 30 mg mL⁻¹ was a reasonable starting concentration in terms of attaining significant amounts of dispersed sheets in aqueous medium, and such concentration was subsequently used throughout the experiments. Lower starting concentrations of the layered compounds yielded correspondingly lower dispersed concentrations, whereas the use of much higher initial concentrations generally failed to increase substantially the concentration of the final suspension.

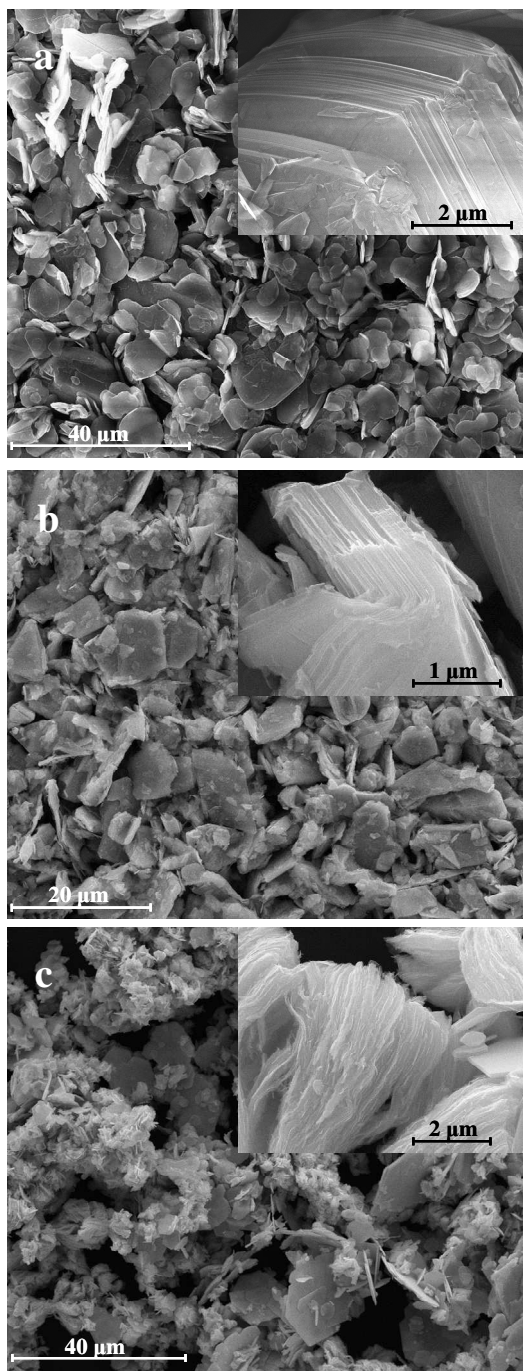


Figure 1. Representative FE-SEM images of the starting powders of (a) h-BN, (b) MoS₂, and (c) WS₂.

The dispersing ability of the surfactants was systematically investigated in a series of benchmark tests that consisted of sonicating the layered materials (30 mg mL⁻¹) in surfactant solutions of different concentrations for 5 h at a power of 26 W L⁻¹ and

finally centrifuging the sonicated suspensions at 1500 rpm for 20 min. The centrifugation conditions were chosen so as to maximize the amount of material that could be suspended in the solution showing no or little amount of precipitation to the naked eye over the course of weeks. The sonication time and power were also selected to favour the production of dispersions with reasonable concentrations. The effect of these two parameters was studied in detail and will be further discussed below. Fig. 2a plots typical UV-vis spectra recorded for the resulting dispersions of h-BN (gray curve), MoS₂ (green) and WS₂ (red) in water with the surfactant Brij 700, which display the expected features for each of these materials.^{19,20} Being a wide bandgap (~6 eV) semiconductor,⁴ h-BN only exhibits strong absorbance at the shortest wavelengths in the measured range. On the other hand, the metal dichalcogenides show well-defined peaks at 612 and 674 nm (MoS₂), and 630 nm (WS₂), which are known to arise from excitonic transitions characteristic of such materials.⁵ After subtracting the background from the MoS₂ and WS₂ spectra (e.g., inset to Fig. 2a for MoS₂), the absorbance of the different dispersions was determined at a specific wavelength (350, 674 and 630 nm for h-BN, MoS₂ and WS₂, respectively) as a relative measure of their concentration. Photographs of the typical aqueous dispersions are shown in Fig. 2b (WS₂), c (MoS₂) and d (h-BN).

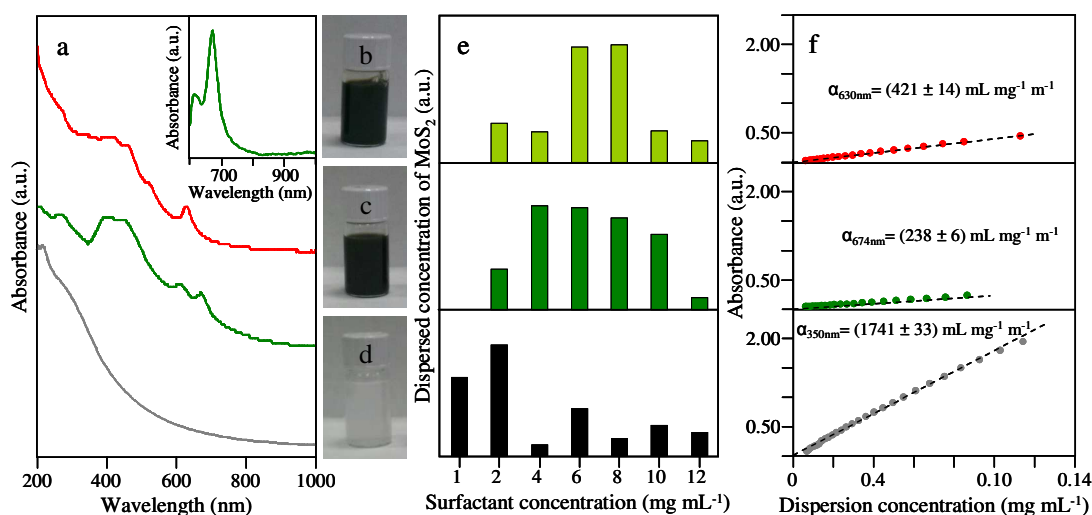


Figure 2. (a) UV-vis spectra recorded for aqueous dispersions of WS₂ (red curve), MoS₂ (green) and h-BN (gray) stabilized by the surfactant Brij 700. Digital photographs of the suspensions are shown in (b) for WS₂, (c) for MoS₂ and (d) for h-BN. (e) Dispersed concentration of MoS₂ as a function of surfactant concentration for SC (light green), Brij700 (dark green) and PVP (black). (f) Calibration plots relating dispersed concentration with absorbance at 630 nm for WS₂ (red circles), 674 nm for MoS₂ (green) and 350 nm for h-BN (gray). For WS₂ and MoS₂, absorbance data are given after subtraction of the scattering background.

On assessing the effect of surfactant concentration on the amount of material that could be successfully dispersed, we observed that in most cases the dispersed concentration went through a maximum value with increasing surfactant concentration. This is exemplified in Fig. 2e for MoS₂ with the surfactants SC, Brij 700 and PVP. A similar behavior has been recently reported for aqueous graphene dispersions with such anionic stabilizers as SC, sodium deoxycholate or several pyrene derivatives.^{26,27} Although the origin of this behavior is not well understood, it has been related to concentration-induced changes in the ionization degree of the stabilizer functional

groups,²⁶ but such a mechanism cannot be expected to be in effect for non-ionic stabilizers. In principle, one could expect the dispersed concentration to steadily increase with surfactant concentration until a plateau value is reached, but the observation of a maximum requires some explanation. In aqueous medium, surfactants provide colloidal stability to hydrophobic particles (h-BN, MoS₂ and WS₂ in the present case) through adsorption of their hydrophobic section onto the particle surface, whereas their hydrophilic head is usually oriented towards the water molecules. It is known that surfactant self-assembly at the particle-water interface can lead to different types of surfactant aggregates, such as full micelles, hemimicelles or monolayers.^{28, 29} Furthermore, for a given surfactant the colloidal stability of the particle depends not only on the amount of surfactant adsorbed at the interface, but also on the specific structure (conformation, orientation, etc) of the formed aggregates.^{30,31}

As a rule, the amount of surfactant adsorbed at a water-solid interface has been shown to remain approximately constant at surfactant concentrations above the critical micelle concentration (cmc).^{30,32} The range of surfactant concentrations investigated here (2-12 mg mL⁻¹) lies above the cmc values of the tested non-ionic surfactants (typically well below 1 mg mL⁻¹),³³ so their amount adsorbed on the layered solids is not expected to change significantly over such a range. For SC, the concentration at which the amount of dispersed solid decreased markedly (around 10 mg mL⁻¹, see Fig. 2e) was also above the cmc value of this surfactant (~4-6 mg mL⁻¹).³⁴ We thus have to conclude that changes in the amount of surfactant adsorbed onto the layered materials are not responsible for the observation of maxima in the dispersed concentrations. Rather, we interpret that these maxima are the result of structural transformations in the adsorbed surfactant layer, which would be associated with changes in the ability of the layer to keep the solid particles colloidally stabilized. Such transformations have been

both theoretically predicted and experimentally observed to occur upon changes in surfactant concentration (including concentrations above the cmc) for some aqueous surfactant-solid systems.^{29,31, 35, 36} However, information regarding the possible arrangements of the adsorbed surfactant layer for the specific systems investigated here is currently not available, so further experimental and/or theoretical work will be required to validate the proposed interpretation.

The surfactant concentrations that yielded maximum dispersed amounts of the layered solids are collected in Table 1 for the different surfactant-solid combinations. These were considered to be the optimal concentrations for each system, and were therefore used in all the subsequent experiments. We note that there is a significant disparity in the obtained values, being as low as 2 mg mL⁻¹ for, e.g., the surfactant Tween 85 with WS₂, and as high as 12 mg mL⁻¹ for P-123 with MoS₂. It is also worth mentioning that for a given surfactant-solid system, the dispersed concentration measured at the optimal surfactant concentration can be very different to that achieved at other concentrations (see, for instance, the cases of SC and PVP with MoS₂ in Fig. 2e). This indicates that in order to compare the actual performance of the surfactants in the colloidal stabilization of these layered materials, we should use the optimal concentration value for each surfactant instead of the same concentration for all surfactants, as has been usually done in previous studies with, e.g., graphene.^{23,24}

Surfactant	MoS ₂		WS ₂		h-BN	
	Surfactant concentration (mg/mL)	Dispersion concentration (mg/mL)	Surfactant concentration (mg/mL)	Dispersion concentration (mg/mL)	Surfactant concentration (mg/mL)	Dispersion concentration (mg/mL)
SC	6	0.38 ± 0.06	10	0.77 ± 0.08	4	0.08 ± 0.02
Brij 30	8	0.5 ± 0.2	8	0.3 ± 0.2	8	0.18 ± 0.03
Brij 700	4	0.52 ± 0.08	10	0.6 ± 0.2	2	0.07 ± 0.01
DBDM	10	1.2 ± 0.4	10	2.9 ± 0.8	2	0.046 ± 0.001
Gum arabic	8	0.4 ± 0.1	4	2.1 ± 0.6	2	0.056 ± 0.005
P-123	12	12 ± 2	10	2.8 ± 0.7	6	0.08 ± 0.03
PVP	2	0.22 ± 0.01	10	0.6 ± 0.1	1	0.110 ± 0.005
Tritón X-100	10	0.6 ± 0.1	8	1.3 ± 0.2	8	0.05 ± 0.02
Tween 80	6	1.5 ± 0.3	6	0.8 ± 0.5	6	0.08 ± 0.01
Tween 85	2	0.25 ± 0.06	2	0.04 ± 0.02	12	0.05 ± 0.01
Water	---	0.004 ± 0.001	---	0.0017 ± 0.0005	---	0.12 ± 0.02
IPA-water (30-70 vol%)	---	0.71 ± 0.02	---	0.78 ± 0.07	---	0.40 ± 0.09

Table 1: Optimal surfactant concentrations and final dispersed concentrations of MoS₂, WS₂ and h-BN exfoliated in water.

To determine the dispersed concentrations attained with the different surfactants in terms of mass of layered material per unit volume from their measured absorbance values, knowledge of the extinction coefficient of each material is first required. To gauge the extinction coefficients, we prepared relatively large amounts of h-BN, MoS₂ and WS₂ dispersed in isopropanol (30 %vol)-water mixtures (see below for the selection of this mixture) by sonicating the materials at an initial concentration of 30 mg mL⁻¹ for 5 h at a power of 25 W L⁻¹ and finally centrifuging at 1500 rpm for 20 min. Then, a

given volume of the resulting dispersions was vacuum-filtered through a polycarbonate membrane filter (50 nm of pore size). The solid collected on the membrane filter was weighed to calculate its concentration in the prepared suspensions. Because no surfactants were employed to prepare such suspensions, the weight of the layered materials could be determined with better accuracy. Finally, a calibration plot relating absorbance at a given wavelength (after background subtraction for MoS₂ and WS₂) and the concentration of suspensions prepared by serially diluting the original suspension in the appropriate solvent was obtained, from which the extinction coefficient of the material could be determined (Fig. 2f). The following values were found: (1741 ± 33) m⁻¹ g⁻¹ L at 350 nm for h-BN, (238 ± 6) m⁻¹ g⁻¹ L at 674 nm for MoS₂ and (421 ± 14) m⁻¹ g⁻¹ L at 630 nm for WS₂. Although such values were obtained from aqueous dispersions in the absence of surfactants and (for MoS₂ and WS₂) in the presence of isopropanol, we assume that they are also essentially valid for surfactant-stabilized aqueous dispersions. This is because only weak interactions between water, isopropanol or surfactant molecules and the layered materials are expected to arise, so the absorption behavior of the latter will not be very significantly altered by such interactions. Likewise, we note that the extinction coefficients estimated for MoS₂ and WS₂ from their background-subtracted spectra are very different (much smaller) to those obtained when the background is not subtracted. For example, the coefficient for MoS₂ without background subtraction would be (2692 ± 51) m⁻¹ g⁻¹ L.

Estimates of dispersed concentrations at the optimal surfactant concentrations are given in Table 1 for the different surfactant-layered material combinations. Significant differences in the amount of material that can be stably suspended by these surfactants are noticed. For instance, the surfactants PVP or Tween 85 appear to be rather inefficient in exfoliating and dispersing MoS₂ in aqueous medium, whereas P-123

affords very high concentrations of this layered material. Similar trends are also observed for WS₂, with Tween 85 being the worst performing surfactant, and DBDM and P-123 being the best ones. For the two metal dichalcogenides, we note that the dispersing efficiency of many of these non-ionic surfactants compares favorably with that of SC, thus confirming the hypothesis that such type of surfactants can be as effective as, or even outperform, ionic ones in their colloidal stabilization. Furthermore, it has been previously reported that certain water-alcohol (e.g., ethanol and isopropanol) mixtures are quite effective media for the exfoliation and stabilization of MoS₂ and WS₂ without requiring the addition of any stabilizers.^{37,38} We therefore prepared dispersions of MoS₂ and WS₂ in isopropanol-water mixtures with the optimal proportion of the alcohol (30 %vol) under the same processing conditions as those used to obtain the surfactant-stabilized suspensions, and compared the results in Table 1. Although the isopropanol-water mixture is rather effective in dispersing significant concentrations of the metal dichalcogenides, it is clearly outperformed by some surfactants. More significantly, the suspensions prepared with the best surfactants generally exhibited long-term colloidal stability, showing no or little sign of sedimentation over the course of at least 6 months. By contrast, most of the material dispersed in the isopropanol-water mixture was seen to precipitate in a matter of days, even if the suspensions were kept in air-tight vials to prevent evaporation of the alcohol.

As shown in Table 1, the results for h-BN were very different to those obtained with MoS₂ and WS₂. First, even though the dispersions were prepared under exactly the same conditions as those used for the metal dichalcogenides, the dispersed concentrations were rather low and relatively similar for all the tested surfactants, i.e., there were no specific surfactants that afforded high concentrations of this material. Second, what was even more surprising was the fact that such concentrations were not better than that

achieved in the absence of surfactants. It has been reported that thin h-BN platelets can be exfoliated and stabilized in water without surfactants through a hydrolytic process induced by sonication.²⁵ This process is thought to lead to the decoration of the edges and basal plane defects of the h-BN platelets with hydroxyl groups, thus conferring the platelets with some hydrophilic character that would be responsible for their colloidal stabilization in water. We speculate that such a hydrophilic character might change the adsorption behavior of the surfactant molecules on the h-BN platelet surface, so that there would no longer be a strong thermodynamic drive for the hydrophobic section of the surfactant molecules to adsorb on the platelet surface. As a result, their ability to stabilize the platelets in water would be significantly hampered. However, we note that the surfactant-free h-BN dispersions are colloidally stable under neutral and basic pH, probably due to electrostatic repulsion effects afforded by ionization of the hydroxyl groups, but precipitate under acidic conditions.²⁵ By contrast, the stabilization provided by many non-ionic surfactants is not drastically affected in acidic medium,³⁹ so their use would still be advantageous when working under such physicochemical conditions.

The effect of sonication time (up to several hours) and power (between ~10 and 50 W L⁻¹) on the dispersed concentrations was also investigated for several surfactant-layered material combinations, and some representative results are shown in Fig. 3. As could be anticipated, the dispersed concentrations tended to increase with sonication time (Fig. 3a), although the magnitude of such increases was seen to differ for different surfactants, reflecting their different dispersing abilities commented upon before, and also between MoS₂/WS₂ and h-BN. For instance, the concentration of dispersed MoS₂ in Tween 80 and of WS₂ in gum arabic rose by ~0.25-0.35 mg per hour, compared with a value of ~0.02 mg per hour for h-BN in PVP. Sonication power should have a strong influence of the dispersed concentrations, but this parameter is usually not considered in

the liquid-phase exfoliation of graphene and other 2D materials.⁴⁰ Indeed, sonication power had a strong effect on the amounts of suspended material that could be obtained here, exhibiting a marked increase with this parameter (Fig. 3b). Albeit the interaction of solid particles with ultrasound waves in a liquid is quite complex and not thoroughly understood, it is generally agreed that the collapse of cavitation bubbles at or near the particle surface generates intense shock waves and liquid microjets that damage the particles.⁴¹ For layered materials, this can be expected to lead to the tearing and exfoliation of small fragments (platelets) from the particle surface, providing that the energy associated to such damage events is above a certain threshold. Indeed, it can be seen from Fig. 3b that the dispersed concentrations fall to nearly zero for sonication powers in the 10-20 W L⁻¹ range. As the sonication power is increased above this range, the number of cavitation bubbles with sufficient energy should rise and/or their energy should increase so as to allow larger numbers of fragments to be ripped apart from the surface of the particles. As a result, the concentration of platelets suspended in the aqueous medium would be expected to increase, as actually observed in Fig. 3b. However, microscopic characterization indicated that higher sonication powers also tended to produce platelets with smaller lateral dimensions, which is an undesirable feature in many cases. In this regard, a reasonable compromise can be attained by selecting relatively modest powers above the 10-20 W L⁻¹ range (e.g., 26 W L⁻¹) without sacrificing drastically the final dispersed concentrations.

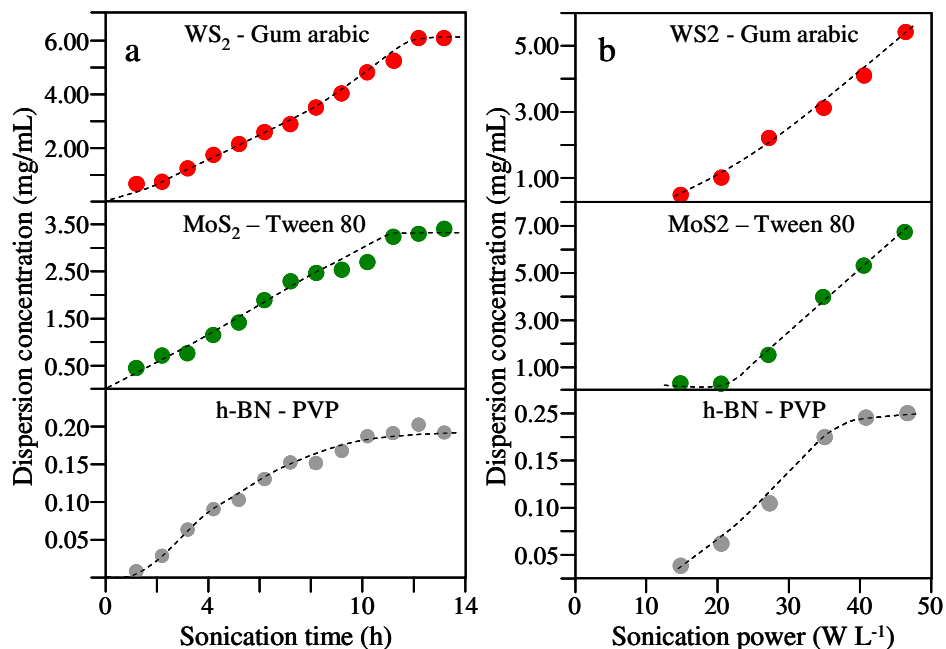


Figure 3. Dispersed concentrations of WS₂ with gum Arabic (red circles), MoS₂ with Tween 80 (green) and h-BN with PVP (gray) as a function of sonication time (a) and power (b).

Although the previous results have demonstrated that the layered materials under investigation can be suspended in water using non-ionic surfactants, with a high efficiency in many cases, the characteristics of the dispersed objects are not known and must be elucidated. In particular, it is desirable that the dispersions are constituted by sheets with a limited number of monolayers and that the sheets have not been structurally or chemically altered to any significant extent by the ultrasonic processing. Fig. 4 shows TEM images of the typical objects that were observed for some representative surfactant-stabilized dispersions: MoS₂ with P-123 (a) and Brij 700 (b), WS₂ with DBDM (c) and Triton X-100 (d), and h-BN with Tween 80 (e and f). We note that some of the features observed in these images appear slightly blurred. We believe the main reason for this to be related to the presence of surfactant molecules on/around

the exfoliated platelets. For example, the rounded shadows seen in the upper part of Fig. 4e can be attributed to surfactant aggregates. As a result, the quality of the images tends to degrade to some extent. It was not easy to remove these surfactant molecules. One possible way to do this would be by aggressively rinsing the sample with water (like we did in the case of AFM imaging), but the Cu grids covered with a thin carbon film that were used for TEM are very fragile and did not stand such a rinsing process. In any case, the quality of the presented images was sufficient to discern its main features. Specifically, the dispersions were seen to be mostly or even exclusively constituted by thin platelets, which were interpreted to be few-layered sheets of the corresponding materials, thereby suggesting that a considerable degree of exfoliation was attained with these surfactants. The platelets displayed irregular polygonal shapes with lateral dimensions approximately between 50 and 300 nm for MoS₂ and WS₂, and 100-500 nm for h-BN. We note that the typical sizes of the h-BN platelets tended to be somewhat larger than those of their MoS₂ and WS₂ counterparts under the same processing conditions. This can be probably put down to differences in tensile strength between h-BN and the metal dichalcogenides, i.e, relatively low strength values for the latter would facilitate breaking-up the exfoliated platelets into smaller fragments during sonication.¹⁷

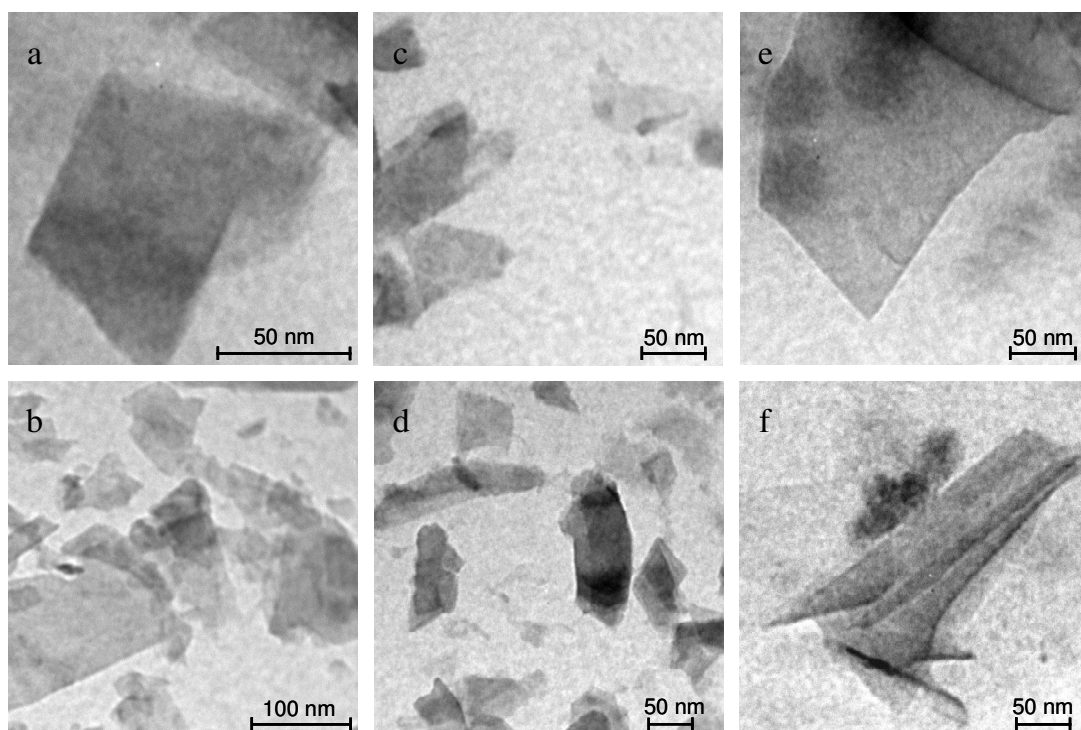


Figure 4. TEM images of representative platelets exfoliated in water via sonication: MoS₂ with P-123 (a) and Brij 700 (b), WS₂ with DBDM (c) and Triton X-100 (d), and h-BN with Tween 80 (e,f).

Platelet thickness was evaluated by means of AFM imaging, as exemplified in Fig. 5 for MoS₂ (a), WS₂ (b) and h-BN (c) with Tween 80. Line profiles such as those shown superimposed on the images of Fig. 5a-c allowed to determine the apparent height of the platelets relative to the supporting substrate, which in turn was taken as an estimate of their thickness. Histograms showing platelet thickness distribution for the samples of Fig. 5a, b and c are presented in Fig. 5d, e and f, respectively. Typical values ranged between 2 and 10 nm for the three Tween 80-stabilized samples, and similar results were obtained for dispersions stabilized with other surfactants. These values are comparable to those reported previously for platelets of the same materials exfoliated in

the liquid phase.^{17,21} Taking into account that the thickness of one monolayer of these materials is about 0.7 nm (MoS₂ and WS₂) and 0.35 nm (h-BN),^{42,43} we deduce that the platelets in the present surfactant-stabilized dispersions would typically contain from about 3 to 14 layers of MoS₂ or WS₂ and from 5 to 25 layers of h-BN. However, as a result of the different nature of the platelets and the supporting substrate, we note that some inaccuracy (instrumental offset) can be introduced in the determination of thickness values by this procedure, which typically amounts to ~1 nm in excess of the actual thickness.⁴⁴⁻⁴⁷ Likewise, the presence of surfactant molecules adsorbed on the platelet surface, which are difficult to remove completely, can also increase the measured thickness values. As a result, the figures provided here probably overestimate the actual platelet thicknesses by the equivalent of up to several monolayers of the material. Another way to determine the thickness (layer number) of the platelets would be by counting the number of lattice fringes observed by TEM at the platelet edges. This has been successfully done in the case of graphene, where folds are usually formed at its edges that facilitate the observation of fringes. However, for transition metal dichalcogenides this approach is much more difficult to implement because the platelets tend to be more rigid than graphene, so that folds do not readily form.¹⁷

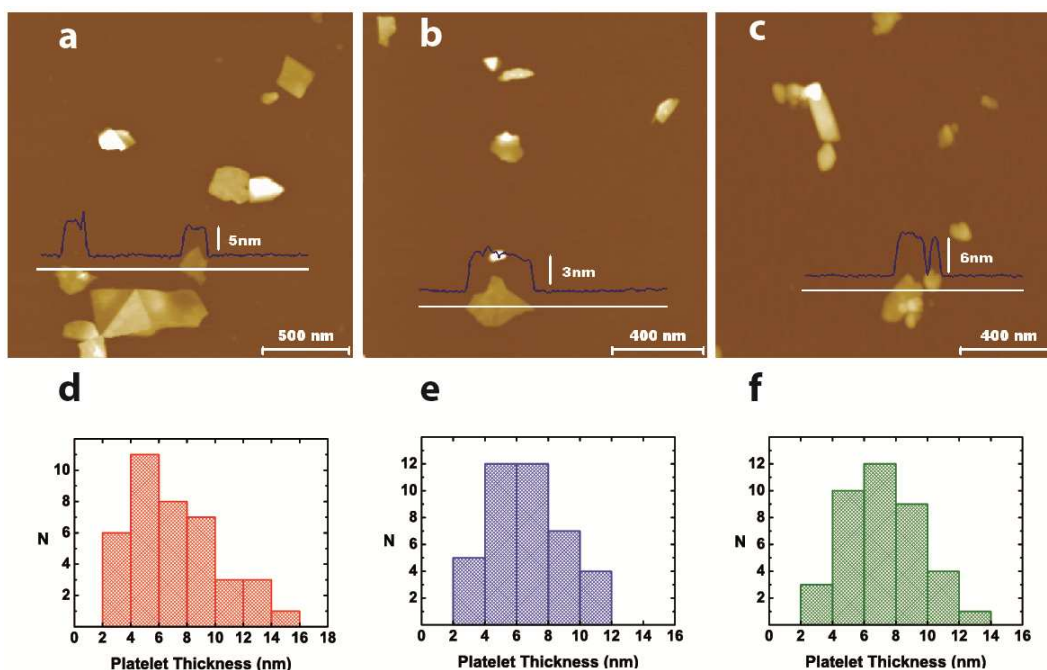


Figure 5. AFM images of platelets exfoliated in water with Tween 80 and deposited onto mica substrates: h-BN (a), MoS₂ (b) WS₂ (c). Line profiles (blue traces) taken along the marked white lines are shown superimposed on the AFM images. Histograms showing the platelet thickness distribution as derived from the apparent height of the platelets in the AFM images: h-BN (d), MoS₂ (e) and WS₂ (f).

Raman spectroscopy was employed to gain structural information on the materials that comprise the aqueous dispersions. Fig. 6 (red traces) shows representative Raman spectra corresponding to aqueous dispersions of h-BN (a), MoS₂ (b) and WS₂ (c) with Tween 80. For comparison, spectra recorded for the starting layered materials in bulk form are also presented (blue traces). The Raman spectrum of bulk h-BN was characterized by a peak at $\sim 1366\text{ cm}^{-1}$, which corresponds to a vibration mode of E_{2g} symmetry associated to in-plane bond-stretching motion of pairs of atoms.⁴⁸ For bulk MoS₂, which possesses trigonal prismatic metal coordination (2H polymorph), the

spectrum was dominated by two first-order peaks located at about 384 and 409 cm^{-1} , ascribed to E_{2g}^1 and A_{1g} phonon modes, respectively.⁴⁹ The former mode arises from opposite in-plane displacements of two S atoms with respect to the metal atom, whereas the A_{1g} mode is associated to out-of-plane vibrations of S atoms in opposite directions. Similar to the case of MoS_2 , the polymorph of WS_2 is 2H, with trigonal prismatic metal coordination, but its Raman spectrum exhibited several peaks other than those corresponding to the E_{2g}^1 ($\sim 356 \text{ cm}^{-1}$) and A_{1g} ($\sim 421 \text{ cm}^{-1}$) modes. These additional peaks have been put down to a series of overtone and combination modes, which arise as a result of the laser excitation (532 nm) being in resonance with the B excitonic transition of WS_2 .⁵⁰ The most significant of these overtone modes is the so-called 2LA(M) peak ($\sim 352 \text{ cm}^{-1}$), which is located very close to the E_{2g}^1 mode and is due to longitudinal acoustic (LA) phonons at the M point of the Brillouin zone.

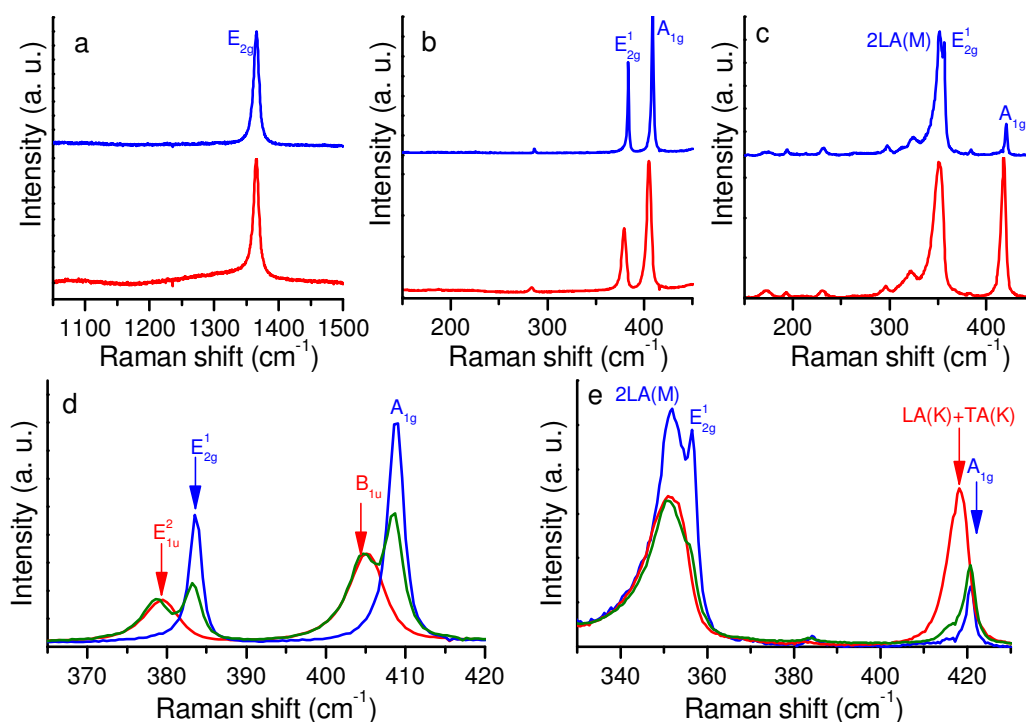


Figure 6. Representative Raman spectra (532 nm laser line) for platelets exfoliated in water with Tween 80 (red trace) and for their non-exfoliated, bulk layered material counterparts (blue): h-BN (a), MoS₂ (b) and WS₂ (c). (d,e) Detailed Raman spectra for MoS₂ (d) and WS₂ (e) recorded for the bulk, non-exfoliated material focusing the laser on basal planes (blue trace) and edges (green) and for the material exfoliated in water by sonication in the presence of Tween 80 (red).

Overall, we see from Fig. 6 that the spectra recorded for platelets of the three layered solids exfoliated and dispersed in water-surfactant media were identical (or almost identical) to those of their bulk counterparts. Such observation suggests that the solids did not undergo any considerable structural changes during their ultrasonic processing or at any other step in the preparation of the dispersions, i.e., the exfoliated platelets generally retained the structural integrity of their parent material. For instance, the exfoliated h-BN platelets exhibited no detectable peaks at ~ 1055 and 1305 cm^{-1} (Fig. 6a, red trace), which would have indicated a partial transformation to the cubic phase of BN.⁴⁸ Likewise, no peaks at about 156 , 226 and 333 cm^{-1} , which would be associated to a distorted 1T phase, were seen to appear for MoS₂ upon exfoliation (Fig. 6b). This phase is known to arise as a result of a structural transformation in 2H-MoS₂ induced by, e.g., lithium intercalation,⁵¹ but such a transformation did not take place in the surfactant-stabilized MoS₂ platelets.

The position of the Raman E_{2g}¹ and A_{1g} peaks in MoS₂ and WS₂ has been recently shown to be sensitive to the number of layers of the specimen.^{49,50,52,53} Similarly, a shift in the frequency of the E_{2g} peak has been predicted to occur when going from bulk to monolayer h-BN,⁵⁴ although to the best of our knowledge this prediction has not yet been experimentally corroborated. Thus, measurement of peak positions could in

principle be used to estimate the number of layers present for samples produced by liquid-phase exfoliation. Nevertheless, the magnitude of the shifts has been shown to be quite small, amounting to just a few cm^{-1} for monolayers and being practically negligible for samples consisting of about 5 or more layers. According to the AFM data (Fig. 5), the surfactant-stabilized platelets prepared here were typically made up of a few to several layers; therefore, we should not expect any significant shifts in the position of their Raman peaks compared with that of their bulk counterparts. This is in fact what we observed for h-BN (Fig. 6a). However, some subtle changes in the position of the observed peaks were noticed for the two metal dichalcogenides. These changes can be better appreciated in the detailed spectra shown in Fig. 6d (MoS_2) and e (WS_2). For exfoliated MoS_2 (Fig. 6d, red trace), peaks at about 379 and 404 cm^{-1} were consistently recorded, which lie $\sim 5 \text{ cm}^{-1}$ lower than those of bulk MoS_2 (Fig. 6d, blue trace) but match against those previously reported for MoS_2 exfoliated in organic solvents.¹⁷ Although a peak at $\sim 404 \text{ cm}^{-1}$ would be consistent with a down-shifted A_{1g} band arising from platelets 1-3 layers thick, if that was the case we should have observed as well an up-shift of the E_{2g}^1 band of about 1-2 cm^{-1} , but not a down-shift.^{49,52} Considering also that the AFM images pointed to exfoliated samples dominated by platelets generally thicker than 1-3 layers, we have to conclude that the origin of the apparent down-shifting of the Raman peaks is not related to platelet thickness. Instead, we propose that it is associated to the presence of a relatively large fraction of edges in the platelets as a result of their small size.

To provide evidence in support of such hypothesis, we note that the type of spectrum shown in Fig. 6d for bulk, non-exfoliated MoS_2 (blue trace) was obtained when the Raman laser was focused onto the basal plane of the MoS_2 particles (see Fig. 1b). However, it was also possible to focus the laser on particle edges, so that the

volume sampled in the Raman measurement contained a majority of atoms in basal planes along with a small, but non-negligible, fraction of atoms at edges. A representative spectrum recorded for the latter situation is shown in Fig. 6d (green trace). Four clearly resolved peaks could be noticed: two of them lay at the same position as that of the E_{2g}^1 and A_{1g} peaks from the basal plane of bulk MoS_2 (~ 384 and 409 cm^{-1} , respectively), whereas the other two matched against the peaks observed for exfoliated MoS_2 (379 and 404 cm^{-1}). This result suggests that the two latter peaks might not be just the E_{2g}^1 and A_{1g} modes down-shifted by 5 cm^{-1} , but instead peaks arising from different vibration modes that become Raman-allowed in the proximity of edges. Indeed, peaks at about 379 and 404 cm^{-1} , together with the E_{2g}^1 and A_{1g} peaks, have been recently reported by Mathew et al for proton-irradiated (i.e., defect-rich) MoS_2 and attributed to E_{1u}^2 and B_{1u} phonon modes that become Raman active when the local symmetry of the lattice is broken (e.g., at vacancies, edges, etc).⁵⁵ Thus, we ascribe the two peaks observed for exfoliated MoS_2 to the E_{1u}^2 and B_{1u} modes. We also infer that such modes tend to yield very intense peaks, because even a quite small fraction of edges can give rise to peaks comparable in intensity to that of the E_{2g}^1 and A_{1g} modes (e.g., green trace in Fig. 6d). For the exfoliated MoS_2 platelets, the fraction of edges should be relatively large on account of their small size ($50\text{-}300\text{ nm}$), so that the E_{1u}^2 and B_{1u} bands can dominate the Raman spectrum altogether (red trace in Fig. 6d). This was also observed for, e.g., MoS_2 dispersions stabilized with surfactants other than Tween 80, such as Brij 700 and PVP (see Fig. S1a in the Electronic Supplementary Information). We observed similar trends, although the down-shifts of the bands were slightly smaller (maxima located at $380\text{-}381\text{ cm}^{-1}$ and $406\text{-}407\text{ cm}^{-1}$) than those of MoS_2 stabilized with Tween 80. We interpret that these features could result from the overlap of E_{2g}^1 and A_{1g} peaks stemming from the basal planes of MoS_2 (maxima at ~ 384 and 409 cm^{-1}) with,

respectively, E_{1u}^2 and B_{1u} peaks stemming from the edges of MoS_2 (379 and 404 cm^{-1}) if they happen to possess similar intensity. Such a situation could arise if Brij 700- and PVP-stabilized dispersions were made up of platelets with slightly larger mean lateral size than that of samples prepared with Tween 80. A detailed investigation of the influence of platelet lateral size on the relative intensity of the E_{1u}^2 and B_{1u} peaks with respect to E_{2g}^1 and A_{1g} peaks is beyond the scope of this work and will be investigated in the future.

A similar reasoning could be applied for the case of WS_2 . For this material, Chung et al have documented the progressive emergence of a peak in the low wavenumber side of the A_{1g} mode (at $\sim 416 \text{ cm}^{-1}$) for WS_2 films that expose increasing fractions of edge planes on their surface.⁵⁶ These authors ascribed the new peak to a combination mode of longitudinal and transverse acoustic phonons [LA(K) + TA(K) mode]. Indeed, we observed such a peak as a shoulder on the A_{1g} band in spectra recorded by focusing the laser on the edges of bulk WS_2 particles (Fig. 6e, green trace), but not when the laser was focused on their basal planes (Fig. 6e, blue trace). Again, this edge-related peak became completely dominant for spectra obtained from the small-sized, exfoliated WS_2 platelets (Fig. 6e, red trace). Likewise, a decrease in the relative intensity of the E_{2g}^1 band could be noticed in Fig. 6e when going from bulk WS_2 (basal plane) to bulk WS_2 (edge) and exfoliated WS_2 . As a general conclusion from the Raman results, we stress that a great deal of caution must be exercised when using peak positions to infer information about the exfoliation degree (thickness) of colloiddally dispersed metal dichalcogenide platelets. Because such platelets tend to display a relatively small lateral size, the characteristics of the observed peaks could be dominated by edge effects rather than by platelet thickness, thus preventing any meaningful assessment of the latter.

Further indication that the exfoliated sheets retained their structural and chemical integrity was obtained by XPS. Fig. 7 shows representative XPS spectra for h-BN (a), MoS₂ (b) and WS₂ (c) in bulk (blue traces) and exfoliated (with Tween 80, red traces) form (further spectra for MoS₂ exfoliated with Brij 700 and PVP can be found in Fig. S1b of the ESI). The binding energies for N 1s and B 1s bands obtained for h-BN in exfoliated form are 398.1 and 190.4 eV, respectively, which are consistent with hexagonal BN.⁵⁷ Furthermore, both the bulk and exfoliated materials show $\pi \rightarrow \pi^*$ shake-up satellites ~9 eV higher than the position of the N 1s and B 1s bands, which are characteristic of sp²-bonded, hexagonal BN,⁵⁷ and are absent in sp³-bonded, cubic BN. Given the similarity between the relative intensity of the satellite to the band in the normalized spectra of bulk and exfoliated h-BN materials, it can be concluded that there has not been any significant transformation from hexagonal to cubic BN with exfoliation, which is consistent with the Raman spectroscopy results. The ~0.6 eV shift in binding energy between the bulk and exfoliated forms of h-BN can be attributed to insufficient charge compensation for the relatively thick pellet of electrically insulating bulk material compared with the very thin film of exfoliated platelets. In the case of MoS₂ (Fig. 7b) and WS₂ (Fig. 7c), a charge effect appears in the spectra of the exfoliated material presumably due to the presence of adsorbed surfactant molecules on the platelets. A hypothetical transformation of a fraction of the starting 2H polymorph into its 1T counterpart upon exfoliation would be accompanied by the development of some asymmetry in the XPS bands for both Mo (or W) and S,¹⁶ which is not observed in the recorded spectra. This suggests that the materials did not undergo any considerable structural changes upon exfoliation, and in fact retain the 2H polymorph of their starting bulk solids.^{16,58}

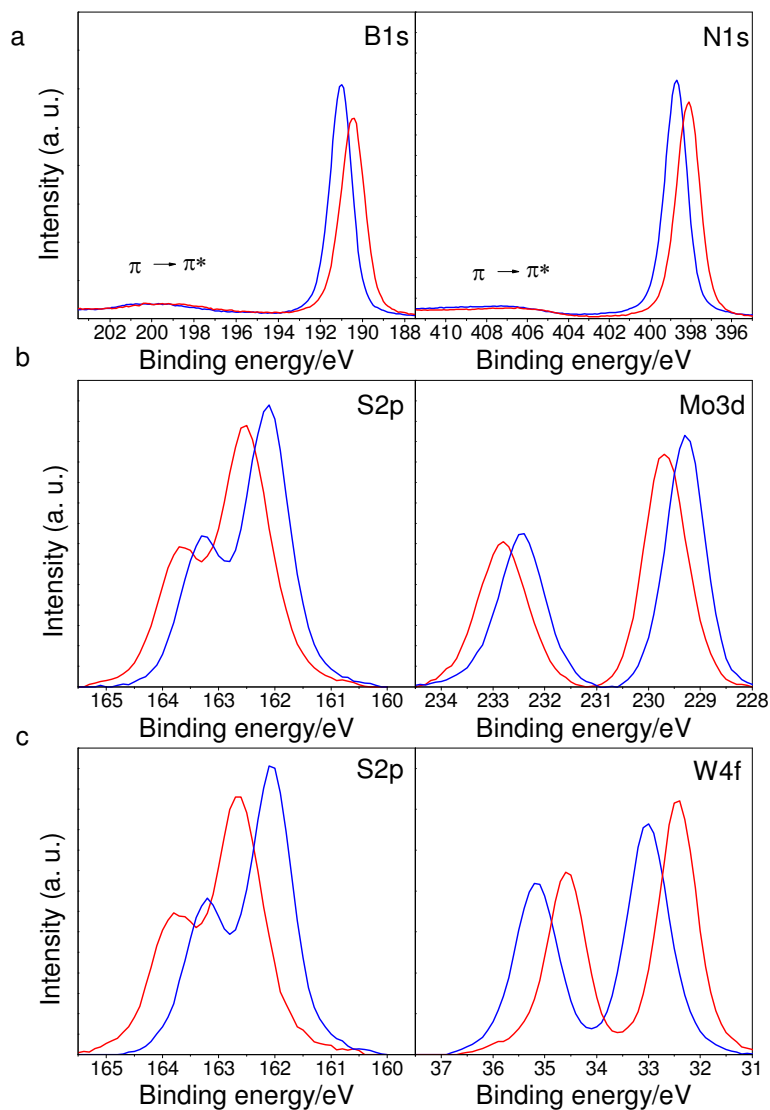


Figure 7. Normalized, high resolution XPS spectra for the non-exfoliated, bulk layered materials (blue traces) and the materials exfoliated in water by sonication in the presence of Tween 80 (red traces): (a) B 1s and N 1s peaks for h-BN, (b) S 2p and Mo 3d peaks for MoS₂, and (c) S 2p and W 4f peaks for WS₂.

Finally, having established the suitability of several non-ionic surfactants for the exfoliation and colloidal stabilization of these layered materials in water, there is a question that is worth posing but often overlooked in the literature: What is the actual amount of surfactant adsorbed on the exfoliated/stabilized platelets? Such a question can be relevant, e.g., when considering practical uses of these platelets. It is well known that the performance of materials and devices obtained from surfactant-stabilized particles can be affected (usually degraded) by the presence of the surfactant molecules.^{26,59} Therefore, knowledge of the amount of surfactant adsorbed on the particles could be helpful in designing materials/devices with improved characteristics. To estimate adsorbed amounts, the aqueous dispersions were centrifuged at a high centrifugal force (20000 *g*) for 120 min to sediment the platelets with their adsorbed surfactant layer, while the non-adsorbed molecules remained in the supernatant liquid. These sediments were then analyzed by thermogravimetry under flowing air. Two representative thermogravimetric plots are shown in Fig. 8 for the sediment of MoS₂ (green plot) and WS₂ (red plot) with P-123. A mass loss step in the ~200-300 °C region signaled the gasification of the surfactant molecules, from which the mass percentage of the latter in the sample could be determined. Values of about 22-29% were obtained, indicating that relatively large amounts of surfactant are required to stabilize the exfoliated platelets in water. However, we note that the sediments could be stably re-dispersed in pure water through a short, mild sonication treatment, thus yielding suspensions with layered material to surfactant concentration ratios of about ~2.4-3.5. Such ratios are significantly higher than the best values reported so far for aqueous dispersions of graphene, h-BN or MoS₂ (~0.3-0.5),^{22,26} making the present re-dispersed suspensions very attractive for the preparation of materials and devices with minimal

interference from the stabilizing agent. Opportunities for application of these dispersions could be found in the biomedical field, due to the good biocompatibility of many non-ionic surfactants, or in photocatalysis, as recently demonstrated for MoS₂ stabilized with P-123.⁶⁰

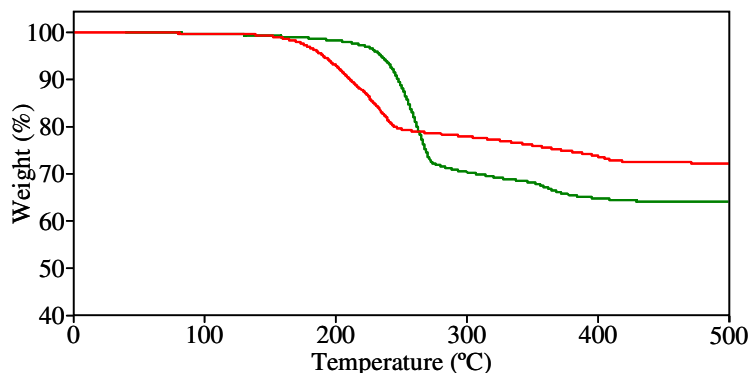


Figure 8. Representative TG plots for centrifuged sediments of MoS₂ (green plot) and WS₂ (red plot) with P-123.

4. Conclusions

We have demonstrated several non-ionic surfactants to be very efficient stabilizers for the production of stable aqueous dispersions of MoS₂ and WS₂ platelets exfoliated by sonication. Concentrations up to several milligrams per milliliter could be achieved, which were considerably higher than those attained for dispersions prepared in two reference media previously reported for their efficacy, namely, water-sodium cholate and water-alcohol in the absence of surfactant. On the other hand, the investigated surfactants were found to be ineffective in affording high concentrations of h-BN platelets. Furthermore, such concentrations were similar to that brought about for this material in water without using surfactants. Although the exact reason for such result is currently unknown, it was tentatively related to chemical changes (decoration with

hydroxyl groups) induced on the platelets by hydrolytic processes during sonication. The Raman spectra for the exfoliated MoS₂ and WS₂ platelets revealed subtle changes relative to the spectra of their bulk counterparts that did not originate from the reduced thickness of the specimens but were instead ascribed to edge effects. This result sends a cautionary tale about the use of Raman spectroscopy as a tool to estimate the thickness of small-sized metal dichalcogenide platelets, such as those produced by sonication-induced exfoliation, which exhibit a relatively large fraction of edges. Finally, aqueous dispersions of MoS₂ and WS₂ with minimal surfactant content (relative to the amount of suspended platelets) could be prepared by re-processing of the as-prepared dispersions, which should facilitate their integration into different materials and devices towards a variety of applications.

Electronic Supplementary Information (ESI)

Additional Raman and XPS spectra of MoS₂ exfoliated in water in the presence of surfactants.

Acknowledgements

Financial support from the Spanish MINECO and the European Regional Development Fund through project MAT2011-26399 is gratefully acknowledged. R.R. is indebted to the Spanish MECED for the receipt of a pre-doctoral (FPU) contract.

References

[1] A. K. Geim and K. S. Novoselov, *Nat. Mater.*, 2007, **6**, 183.

- [2] K. S. Novoselov, V. I. Fal'ko, L. Colombo, P. R. Gellert, M. G. Schwaband and K. Kim, *Nature*, 2012, **490**, 192.
- [3] A. K. Geim, *Science*, 2009, **324**, 1530.
- [4] M. Xu, T. Liang, M. Shi and H. Chen, *Chem. Rev.*, 2013, **113**, 3766.
- [5] S. Z. Butler, S. M. Hollen, L. Cao, Y. Cui, J. A. Gupta, H. R. Gutiérrez, T. F. Heinz, S. S. Hong, J. Huang, A. F. Ismach, E. Johnston-Halperin, M. Kuno, V. V. Plashnitsa, R. R. D. Robinson, R. S. Ruoff, S. Salahuddin, J. Shan, L. Shi, M. G. Spencer, M. Terrones, W. Windl and J. E. Goldberger, *ACS Nano*, 2013, **7**, 2898.
- [6] X. Song, J. Hu and H. Zeng, *J. Mater. Chem. C*, 2013, **1**, 2952.
- [7] M. Chhowalla, H. S. Shin, G. Eda, L. -J. Li, K. P. Loh and H. Zhang, *Nat. Chem.*, 2013, **5**, 263.
- [8] X. Huang, Z. Zeng and H. Zhang, *Chem. Soc. Rev.*, 2013, **42**, 1934.
- [9] S. Park and R. S. Ruoff, *Nat. Nanotech.*, 2009, **4**, 217.
- [10] F. Bonaccorso, A. Lombardo, T. Hasan, Z. Sun, L. Colombo and A. C. Ferrari *Mater. Today*, 2012, **15**, 564.
- [11] M. Cai, D. Thorpe, A. H. Adamson and H. C. Schniepp, *J. Mater. Chem.*, 2012, **22**, 24992.
- [12] V. Nicolosi, M. Chhowalla, M. G. Kanatzidis, M. S. Strano and J. N. Coleman, *Science*, 2013, **340**, 1226419.
- [13] E. Benavente, M. A. Santa Ana, F. Mendizábal and G. González, *Coord. Chem. Rev.*, 2002, **224**, 87.
- [14] H. S. S. R. Matte, A. Gomathi, A. K. Manna, D. J. Late, R. Datta, S. K. Pati and C. N. R. Rao, *Angew. Chem. Int. Ed.*, 2010, **49**, 4059.

- [15] Z. Zeng, Z. Yin, X. Huang, H. Li, Q. He, G. Lu, F. Boey and H. Zhang, *Angew. Chem. Int. Ed.*, 2011, **50**, 11093.
- [16] G. Eda, H. Yamaguchi, D. Voiry, T. Fujita, M. Chen and M. Chhowalla, *Nano Lett.*, 2011, **11**, 5111.
- [17] J. N. Coleman, M. Lotya, A. O'Neill, S. D. Bergin, P. J. King, U. Khan, K. Young, A. Gaucher, S. De, R. J. Smith, I. V. Shvets, S. K. Arora, G. Stanton, H. -Y. Kim, K. Lee, G. T. Kim, G. S. Duesberg, T. Hallam, J. J. Boland, J. J. Wang, J. F. Donegan, J. C. Grunlan, G. Moriarty, A. Shmeliov, R. J. Nicholls, J. M. Perkins, E. M. Grievson, K. Theuwissen, D. W. McComb, P. D. Nellist and V. Nicolosi, *Science*, 2011, **331**, 568.
- [18] G. Cunningham, M. Lotya, C. S. Cucinotta, S. Sanvito, S. D. Bergin, R. Menzel, M. S. P. Shaffer and J. N. Coleman, *ACS Nano.*, 2012, **6**, 3468.
- [19] R. J. Smith, P. J. King, M. Lotya, C. Wirtz, U. Khan, S. De, A. O'Neill, G. S. Duesberg, J. C. Grunlan, G. Moriarty, J. Chen, J. Wang, A. I. Minett, V. Nicolosi and J. N. Coleman, *Adv. Mater.* 2011, **23**, 3944.
- [20] Y. Ge, J. Wang, Z. Shi and J. Yin, *J. Mater. Chem.*, 2012, **22**, 17619.
- [21] X. Chen, R. A. Boulos, P. K. Eggers and C. L. Raston, *Chem. Commun.*, 2012, **48**, 11407.
- [22] F. Zhang, X. Chen, R. A. Boulos, F. M. Yasin, H. Lu, C. Raston and H. Zhang *Chem. Commun.*, 2013, **49**, 4845.
- [23] L. Guardia, M. J. Fernández-Merino, J. I. Paredes, P. Solís-Fernández, S. Villar-Rodil, A. Martínez-Alonso and J. M. D. Tascón, *Carbon*. 2011, **49**, 1653.
- [24] J. -W. T. Seo, A. A. Green, A. L. Antaris and M. C. Hersam, *J. Phys. Chem. Lett.*, 2011, **2**, 1004.

- [25] Y. Lin, T. V. Williams, T. -B. Xu, W. Cao, H. E. Elsayed-Ali and J. W. Connell, *J. Phys. Chem. C.*, 2011, **115**, 2679.
- [26] D. Parviz, S. Das, H. S. T. Ahmed, F. Irin, S. Bhattacharia and M. J. Green, *ACS Nano.*, 2012, **6**, 8857.
- [27] P. Ramalingam, S. T. Pusuluri, S. Periasamy, R. Veerabahu and J. Kulandaivel, *RSC Adv.*, 2013, **3**, 2369.
- [28] L. M. Grant, F. Tiberg and W. A. Ducker, *J. Phys. Chem. B.*, 1998, **102**, 4288.
- [29] R. A. Johnson and R. Nagarajan, *Colloid Surf. A-Physicochem. Eng. Asp.*, 2000, **167**, 31.
- [30] P. Somasundaran, S. C. Mehta, X. Yu and S. Krishnakumar, in *Handbook of Surface and Colloid Chemistry*, CRC Press, Boca Raton, 3rd edn., 2009, ch. 6, pp. 155-196.
- [31] H. Kawasaki, K. Ban and H. Maeda, *J. Phys. Chem. B*, 2004, **108**, 16746.
- [32] S. Paria and K. C. Khilar, *Adv. Colloid Interface Sci.*, 2004, **110**, 75.
- [33] H. -J. Butt, K. Graf and M. Kappl in *Physics and Chemistry of Interfaces*, Wiley-VCH, Weinheim, 2003.
- [34] S. Reis, C. G. Moutinho, C. Matos, B. de Castro, P. Gameiro and J. L. F. C. Lima, *Anal. Biochem.*, 2004, **334**, 117.
- [35] H. N. Patrick, G. G. Warr, S. Manne and I. A. Aksay, *Langmuir*, 1997, **13**, 4349.
- [36] H. Domínguez, *J. Phys. Chem. B.*, 2011, **115**, 12422.
- [37] K. -G. Zhou, N. -N. Mao, H. -X. Wang, Y. Peng and H. -L. Zhang, *Angew. Chem. Int. Ed.*, 2011, **50**, 10839.
- [38] U. Halim, C. R. Zheng, Y. Chen, Z. Lin, S. Jiang, R. Cheng, Y. Huang and X. Duan, *Nature Commun.*, 2013, **4**, 2213.

- [39] M. J. Fernández-Merino, J. I. Paredes, S. Villar-Rodil, L. Guardia, P. Solís-Fernández, D. Salinas-Torres, D. Cazorla-Amorós, E. Morallón, A. Martínez-Alonso and J. M. D. Tascón, *Carbon*, 2012, **50**, 3184.
- [40] A. Ciesielski and P. Samori, *Chem. Soc. Rev.*, 2014, **43**, 381.
- [41] G. Cravotto, and P. Cintas, *Chem. Eur. J.*, 2010, **16**, 5246.
- [42] D. Pacile, J. C. Meyer, Ç. Ö. Girit and A. Zettl, *Appl. Phys. Lett.*, 2008, **92**, 133107.
- [43] H. Li, G. Lu, Z. Yin, Q. He, H. Li, Q. Zhang and H. Zhang, *Small*, 2012, **8**, 682.
- [44] P. Nemes-Incze, Z. Osváth, K. Kamarás and L. P. Biró, *Carbon*, 2008, **46**, 1435.
- [45] P. Solís-Fernández, J. I. Paredes, S. Villar-Rodil, A. Martínez-Alonso and J. M. D. Tascón, *Carbon*, 2010, **48**, 2657.
- [46] A. Castellanos-Gomez, N. Agrait and G. Rubio-Bollinger, *Appl. Phys. Lett.*, 2010, **96**, 213116.
- [47] Y. -H. Lee, K. -K. Liu, A. -Y. Lu, C. -Y. Wu; C. -T. Lin, W. Zhang, C. -Y. Su, C. -L. Hsu, T. -W. Lin, K. -H. Wei, Y. Shi and L. -J. Li, *RSC Adv.*, 2012, **2**, 111.
- [48] S. Reich, A. C. Ferrari, R. Arenal, A. Loiseau, I. Bello and J. Robertson, *Phys. Rev. B.*, 2005, **71**, 205201.
- [49] H. Li, Q. Zhang, C. C. R. Yap, B. K. Tay, T. H. T. Edwin, A. Olivier and D. Baillargeat, *Adv. Funct. Mater.*, 2012, **22**, 1385.
- [50] W. Zhao, Z. Ghorannevis, K. K. Amara, J. R. Pang, M. Toh, X. Zhang, C. Kloc, P. H. Tan and G. Eda, *Nanoscale*, 2013, **5**, 9677.
- [51] S. J. Sandoval, D. Yang, R. F. Frindt and J. C. Irwin, *Phys. Rev. B*, 1991, **44**, 3955.
- [52] D. J. Late, B. Liu, H. S. S. R. Matte, C. N. R. Rao and V. P. Dravid, *Adv. Funct. Mater.*, 2012, **22**, 1894.

- [53] A. Berkdemir, H. R. Gutiérrez, A. R. Botello-Méndez, N. Perea-López, A. L. Elías, C. -I. Chia, B. Wang, V. H. Crespi, F. López-Urías, J. -C. Charlier, H. Terrones and M. Terrones, *Sci. Rep.*, 2013, **3**, 1755.
- [54] R. Arenal, A. C. Ferrari, S. Reich, L. Wirtz, J. -Y. Mevellec, S. Lefrant, A. Rubio and A. Loiseau, *Nano Lett.*, 2006, **6**, 1812.
- [55] S. Mathew, K. Gopinadhan, T. K. Chan, X. J. Yu, D. Zhan, L. Cao, A. Rusydi, M. B. H. Breese, S. Dhar, Z. X. Shen, T. Venkatesan and J. T. L. Thong, *Appl. Phys. Lett.*, 2012, **101**, 102103.
- [56] J. -W. Chung, Z. R. Dai, K. Adib and F. S. Ohuchi, *Thin Solid Films*, 1998, **335**, 106.
- [57] K. S. Park, D. Y. Lee, K. J. Kim and D. W. Moon, *Appl. Phys. Lett.*, 1997, **70**, 315.
- [58] A. P. Shpak, A. M. Korduban, L. M. Kulikov, T. V. Kryshchuk, N. B. Konig and V. O. Kandyba, *J. Electron Spectrosc. Relat. Phenom.*, 2010, **181**, 234.
- [59] Y. Wang, C. Di, Y. Liu, H. Kajiura, S. Ye, L. Cao, D. Wei, H. Zhang, Y. Li and K. Noda, *Adv. Mater.*, 2008, **20**, 4442.
- [60] M. D. J. Quinn, N. H. Ho and S. M. Notley, *ACS Appl. Mater. Interfaces*, 2013, **5**, 1275.

Captions to table

Table 1: Optimal surfactant concentration and dispersed concentration at the optimal surfactant concentration for the different surfactant- layered materials combinations.

Captions to figures

Figure 1. Representative FE-SEM images of the starting powders of (a) h-BN, (b) MoS₂, and (c) WS₂.

Figure 2. (a) UV-vis spectra recorded for aqueous dispersions of WS₂ (red curve), MoS₂ (green) and h-BN (gray) stabilized by the surfactant Brij 700. Digital photographs of the suspensions are shown in (b) for WS₂, (c) for MoS₂ and (d) for h-BN. (e) Dispersed concentration of MoS₂ as a function of surfactant concentration for SC (light green), Brij700 (dark green) and PVP (black). (f) Calibration plots relating dispersed concentration with absorbance at 630 nm for WS₂ (red circles), 674 nm for MoS₂ (green) and 350 nm for h-BN (gray). For WS₂ and MoS₂, absorbance data are given after subtraction of the scattering background.

Figure 3. Dispersed concentrations of WS₂ with gum Arabic (red circles), MoS₂ with Tween 80 (green) and h-BN with PVP (gray) as a function of sonication time (a) and power (b).

Figure 4. TEM images of representative platelets exfoliated in water via sonication: MoS₂ with P-123 (a) and Brij 700 (b), WS₂ with DBDM (c) and Triton X-100 (d), and h-BN with Tween 80 (e,f).

Figure 5. AFM images of platelets exfoliated in water with Tween 80 and deposited onto mica substrates: h-BN (a), MoS₂ (b) WS₂ (c). Line profiles (blue traces) taken along the marked white lines are shown superimposed on the AFM images. Histograms showing the platelet thickness distribution as derived from the apparent height of the platelets in the AFM images: h-BN (d), MoS₂ (e) and WS₂ (f).

Figure 6. Representative Raman spectra (532 nm laser line) for platelets exfoliated in water with Tween 80 (red trace) and for their non-exfoliated, bulk layered material counterparts (blue): h-BN (a), MoS₂ (b) and WS₂ (c). (d,e) Detailed Raman spectra for MoS₂ (d) and WS₂ (e) recorded for the bulk, non-exfoliated material focusing the laser on basal planes (blue trace) and edges (green) and for the material exfoliated in water by sonication in the presence of Tween 80 (red).

Figure 7. Normalized, high resolution XPS spectra for the non-exfoliated, bulk layered materials (blue traces) and the materials exfoliated in water by sonication in the presence of Tween 80 (red traces): (a) B 1s and N 1s peaks for h-BN, (b) S 2p and Mo 3d peaks for MoS₂, and (c) S 2p and W 4f peaks for WS₂.

Figure 8. Representative TG plots for centrifuged sediments of MoS₂ (green plot) and WS₂ (red plot) with P-123.

Production of aqueous dispersions of inorganic graphene analogues by exfoliation and stabilization with non-ionic surfactants

Laura Guardia, Juan I. Paredes, Rubén Rozada, Silvia Villar-Rodil, Amelia Martínez-Alonso, Juan M. D. Tascón

Instituto Nacional del Carbón, INCAR-CSIC, Apartado 73, 33080 Oviedo, Spain

The production of stable aqueous suspensions of several inorganic graphene analogues was performed by exfoliation of the corresponding bulk layered materials via sonication using non-ionic surfactants as dispersing agents.

